

Optimal Position and Target Rate for Covert Communication in UAV-Assisted Uplink RSMA Systems

Zhengxiang Duan ¹, Xin Yang ^{1,*}, Tao Zhang ² and Ling Wang ^{1,*}¹ School of Electronics and Information, Northwestern Polytechnical University, Xi'an 710072, China² China Academy of Launch Vehicle Technology, Beijing 100076, China

* Correspondence: xinyang@nwpu.edu.cn (X.Y.); lingwang@nwpu.edu.cn (L.W.)

Abstract: With the explosive increase in demand for wireless communication, the issue of wireless communication security has also become a growing concern. In this paper, we investigate a novel covert communication for unmanned aerial vehicle (UAV)-assisted uplink rate-splitting multiple access (RSMA) systems, where a UAV adopts the rate-splitting (RS) strategy to increase the total transmission rate while avoiding deteriorating the covert transmission of a ground user. In the proposed system, a ground user and a UAV adopt the RSMA scheme to simultaneously communicate with a base station surveilled by an evil monitor. The UAV acts as both the transmitter and the friendly jammer to cover the ground user's transmission with random power. To maximize the expected sum rate (ESR), we first study the RS strategy and obtain the optimal power allocation factor. Then, the closed-form of minimum detection error probability (DEP), ESR, and optimal target rate of the UAV are derived. Constrained by the minimum DEP and expected covert rate (ECR), we maximize the ESR by optimizing the position and target rate of the UAV. Numerical results show that the proposed scheme outperforms the traditional NOMA systems in terms of ESR with the same DEP and ECR.

Keywords: covert communication; RSMA; UAV; sum rate



Citation: Duan, Z.; Yang, X.; Zhang, T.; Wang, L. Optimal Position and Target Rate for Covert Communication in UAV-Assisted Uplink RSMA Systems. *Drones* **2023**, *7*, 237. <https://doi.org/10.3390/drones7040237>

Academic Editor: Maurizio Magarini

Received: 6 March 2023

Revised: 24 March 2023

Accepted: 27 March 2023

Published: 28 March 2023



Copyright: © 2023 by the authors. Licensee MDPI, Basel, Switzerland. This article is an open access article distributed under the terms and conditions of the Creative Commons Attribution (CC BY) license (<https://creativecommons.org/licenses/by/4.0/>).

1. Introduction

The rapid development of intelligent wireless terminals promotes a large amount of wireless private information, bringing broader attention to information security. The study of communication security at the physical layer has been segregated into two directions, namely physical layer security (PLS) [1,2] and covert communications [3,4]. The purpose of PLS is to ensure that the transmitted information is not intercepted by eavesdroppers, i.e., protecting the transmitted content. However, it's not always sufficient to focus solely on protecting information security, as the exposure of communication behavior can also pose potential risks and threats. For example, the exposure of the signal transmission would disclose the existence and position of a device to an adversary, ultimately resulting in an attack on the device. Different from PLS, covert communications focus on shielding the transmission behavior from potential watchful adversaries. Bash et al. initiated covert communication research and proposed a square root law as the fundamental limit in the additive white Gaussian noise (AWGN) channels [3]. In [4], the authors proved that it is possible to transmit $\mathcal{O}(n)$ bits covertly and reliably in n uses of AWGN channel when the monitor has uncertainty about the received power.

With the growing number of connected devices and increasing data traffic, there is a need for more efficient and effective ways to manage the available resources. Non-orthogonal multiple access (NOMA) is a promising technique that offers improvements over conventional orthogonal multiple access techniques in terms of spectral efficiency [5,6]. In [7], the PLS in NOMA systems assisted with a HAP and UAVs was studied. Rate-splitting multiple access (RSMA), which can further increase the sum rate, has recently

emerged as a more general and robust transmission framework compared to NOMA [8–12]. In particular, the performances of uplink RSMA systems were studied in [10,11]. In [10], the authors investigated a rate-splitting (RS) strategy in uplink cognitive radio systems, where a secondary user splits its rate to guarantee the primary user's transmission. In [11], the optimal decoding order and maximum sum rate in uplink RSMA systems were studied. To protect the privacy information, the authors in [13] studied the security and energy efficiency of the cognitive RSMA-based satellite-terrestrial networks, where a beamforming scheme was proposed to prevent eavesdropping and increase energy efficiency.

Covert communications in NOMA systems have also been widely studied [14,15]. The author in [14] achieved covert communication in an uplink NOMA system via random power jamming generated by channel inversion power control. The study in [15] explored an intelligent reflecting surface (IRS)-assisted covert communication in both downlink and uplink NOMA systems. The randomness was brought about by the phase-shift uncertainty of IRS and the overlapping signal transmission. In addition, unmanned aerial vehicles (UAVs) have been used by virtue of their high mobility, which provides new degrees of freedom to enhance the covertness of communications [16,17]. In [16], the optimal transmit power and location for the UAV were studied to achieve covert communications. In [17], the authors used the geometric method to solve the trajectory problem. Most recently, covert communication in UAV-aided NOMA systems was investigated in [18].

To further increase the sum rate, we investigate covert communication in UAV-assisted uplink RSMA systems in this paper. In this system, a ground user and a UAV simultaneously communicate with a base station (BS), suffering the surveillance of an evil monitor. The UAV acts as both the transmitter and the friendly jammer, covering the ground user's transmission with random power. This work aims to maximize the expected sum rate (ESR) by designing the UAV's power allocation, position, and target rate while guaranteeing the ground user's covertness and throughput. The main contributions of this paper are given as follows.

- We investigate a novel application of RSMA systems, where a UAV splits its rate to avoid deteriorating the covert transmission of a ground user while increasing the ESR. To the best of the authors' knowledge, this is the first work that studied the covert communication in UAV-assisted uplink RSMA system.
- We derive the closed-form expressions of the ESR and obtain the optimal target rate of UAV which maximizes the ESR of the system. Subjected to minimum detection error probability (DEP) and expected covert rate (ECR) constraints, a joint position and target rate optimization problem is formulated for maximizing the ESR of uplink RSMA systems.
- The numerical results show that the proposed scheme outperforms NOMA systems in terms of ESR with the same DEP and ECR and illustrate the effect of constraints on the ESR.

2. System Model

2.1. Communication Scenario

We consider the covert communication in uplink RSMA system, which consists of a pair of RSMA users (U1 and U2), a BS, and a warden (Willie), as shown in Figure 1. U1 is a UAV deployed as both the communication node and the friendly jammer hovering at the constant altitude z_1 . U2 wants to transmit covertly detected by Willie, who continuously senses whether U2 is transmitting by a radiometer. In order to increase the total transmission rate while protecting U2's covert communication, U1 adopts the RS strategy with random transmit power. Without loss of generality, we use a three-dimensional (3D) Cartesian coordinate system to describe locations. Each node is equipped with a single antenna.

Denote $\mathbf{q}_1 = [x_1, y_1, z_1]$, $\mathbf{q}_2 = [x_2, y_2, 0]$, $\mathbf{q}_b = [0, 0, z_b]$, and $\mathbf{q}_w = [x_w, y_w, 0]$ as the coordinate of U1, U2, BS and Willie, respectively. Considering an open area, the communication channel between BS and U2 is modeled as line-of-sight (LOS) links and AWGN

channels. This assumption is based on the fact that in the urban macro, the probability of the LOS path is much higher than that of the non-LOS path when the horizontal distance between BS and terminals is less than 70 m according to 3GPP specification [19]. In addition, we assume that the channels between UAV and terrestrial nodes are mainly dominated by LOS components and the non-LOS path is negligible (as in e.g., [16,17,20]). U2 and Willie are ground users and the channel undergoes the block quasi-static fading, which means that the channel coefficients remain constant in one time slot, and change independently from one time slot to another. The large-scale fading coefficient from node i to node j is denoted as $L_{ij} = \beta_0 \|\mathbf{q}_i - \mathbf{q}_j\|^{-\beta}$, where $i \in \{1,2\}$, $j \in \{b,w\}$, β_0 is the fading coefficient at the reference distance of 1 m, $\beta = 2$ is the free space path-loss factor, and $\|\cdot\|$ denotes the Euclidean norm. And the small-scale fading between U2 and Willie r_{2w} follows complex Gaussian distribution $\mathcal{CN}(0, 1)$. Therefore, the channel coefficient is denoted as

$$h_{ij} = \begin{cases} \sqrt{L_{ij}}, & ij \in \{1w, 1b, 2b\}, \\ \sqrt{L_{ij}}r_{2w}, & ij = 2w. \end{cases} \quad (1)$$

And the channel power gain is expressed by $g_{ij} = |h_{ij}|^2$. Suppose the location information is available for all nodes since Willie's location can be detected with a radar or camera by U1. This assumption has been also widely adopted in previous research on UAV-assisted covert communication [16,17,20]. In addition, we assume that full channel state information (CSI) is available for Willie, while legitimate users only possess statistical CSI between U2 and Willie.

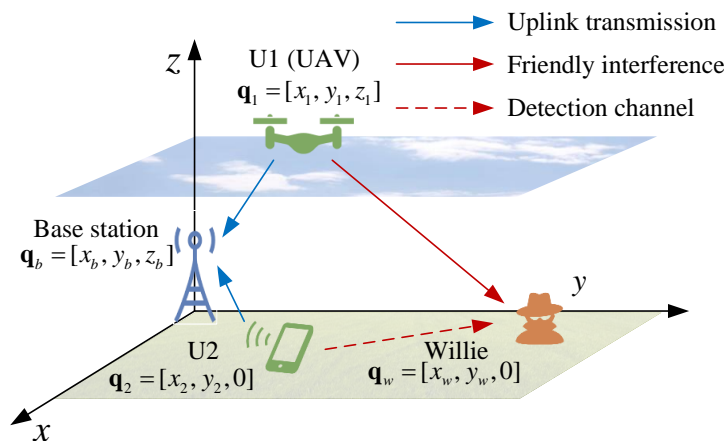


Figure 1. The uplink RSMA covert communication system model.

2.2. Proposed Transmission Scheme

U1 adopts the RS strategy with random transmit power to assist U2's covert and reliable transmission. U2 conveys secret messages at a fixed rate and probability of 0.5, while U1 transmits public information. To confuse Willie's detection, U1 adopts the random transmit power. Furthermore, U1 shares the same resource block with U2 while preventing U2's outage probability from deteriorating through an RS strategy.

Denoting P_i , s_i , and \hat{R}_i as the transmit power, messages, and target rate of U_i , respectively. For simplicity, we adopt μ_i to represent $2^{\hat{R}_i} - 1$. U2 transmits with a fixed power P_2 and rate \hat{R}_2 . Then, the interference threshold of U1 is given by

$$\tau = \frac{g_{2b}P_2}{\mu_2} - \sigma_b^2, \quad (2)$$

where σ_b^2 represents the received noise power at BS. When the interference received by U2 is lower than τ , there is no outage. Conversely, U2's connection is always interrupted when the interference is large than τ . Note that to ensure $\tau \geq 0$, we have $\mu_2 \leq \frac{g_{2b}P_2}{\sigma_b^2}$.

To enhance the covertness of U2’s transmission, P_1 changes from slot to slot, following a continuous uniform distribution within $[P_1^{\min}, P_1^{\max}]$. The probability density function of P_1 is given by

$$f_{P_1}(x) = \begin{cases} \frac{1}{P_1^{\max} - P_1^{\min}}, & \text{if } P_1^{\min} \leq x \leq P_1^{\max}, \\ 0, & \text{otherwise.} \end{cases} \quad (3)$$

In order to obfuscate Willie’s detection and transmit more information, U1 continuously sends messages to BS. The random transmit power of U1 is designed to create ambiguity in Willie’s received power. Consequently, it becomes challenging for Willie to determine whether the increase in received power is due to U2’s transmission or simply a variation in U1’s transmit power.

To increase the total throughput without causing interruptions to U2, U1 applies RS in each time slot. In uplink RSMA systems, U1 needs to split its messages \mathbf{s}_1 into two parts \mathbf{s}_{11} and \mathbf{s}_{12} , as shown in Figure 2a. Note that Figure 2a depicts only one possible splitting scheme. There are also alternative approaches that can be considered. And the received signals at node j can be expressed as

$$\mathbf{y}_j[n] = \begin{cases} \sqrt{P_1}h_{1j}(\sqrt{\alpha}\mathbf{s}_{11}[n] + \sqrt{1-\alpha}\mathbf{s}_{12}[n]) + \mathbf{n}_j[n], & \mathcal{H}_0, \\ \sqrt{P_1}h_{1j}(\sqrt{\alpha}\mathbf{s}_{11}[n] + \sqrt{1-\alpha}\mathbf{s}_{12}[n]) + \sqrt{P_2}h_{2j}\mathbf{s}_2[n] + \mathbf{n}_j[n], & \mathcal{H}_1, \end{cases} \quad (4)$$

where $n = 1 \dots N$ is the index of channel use, $\mathbf{n}_j[n]$ is the received AWGN at j with the variance of σ_j^2 , and α is the power allocation factor satisfying $0 \leq \alpha \leq 1$. The hypotheses \mathcal{H}_1 and \mathcal{H}_0 represent the existence and non-existence of U2’s secret transmission, respectively. It is assumed that $\mathbf{s}_k, k \in \{1, 2, 11, 12\}$, is independently coded with the Gaussian codebook satisfying $\mathbb{E}\{\mathbf{s}_k[n]\mathbf{s}_k^*[n]\} = 1$, where $\mathbb{E}\{\cdot\}$ and $(\cdot)^*$ represent the expectation and conjugate transpose operators, respectively.

The decoding order for uplink RSMA is $\mathbf{s}_{11} \rightarrow \mathbf{s}_2 \rightarrow \mathbf{s}_{12}$ [11]. Thus, the signal-to-interference-plus-noise ratios (SINRs) for BS decoding \mathbf{s}_{11} , \mathbf{s}_2 , and \mathbf{s}_{12} are given by $\gamma_{11} = \frac{\alpha g_{1b} P_1}{g_{2b} P_2 + (1-\alpha)g_{1b} P_1 + \sigma_b^2}$, $\gamma_2 = \frac{g_{2b} P_2}{(1-\alpha)g_{1b} P_1 + \sigma_b^2}$, and $\gamma_{12} = \frac{(1-\alpha)g_{1b} P_1}{\sigma_b^2}$, respectively. Correspondingly, the achievable rates of \mathbf{s}_{11} , \mathbf{s}_2 , and \mathbf{s}_{12} are expressed as $R_{11} = \log_2(1 + \gamma_{11})$, $R_2 = \log_2(1 + \gamma_2)$ and $R_{12} = \log_2(1 + \gamma_{12})$, respectively.

To maximize the sum rate for the RS strategy, U1 needs to allocate the maximum possible power to \mathbf{s}_{12} . As per γ_{12} , \mathbf{s}_{12} is free from interference, hence allocating power to \mathbf{s}_{12} would be more efficient compared to \mathbf{s}_{11} . Considering that the interference received by U2 should be no large than τ to keep U2 uninterrupted, we have $(1-\alpha)g_{1b} P_1 \leq \tau$. Obviously, the allowed maximum power of \mathbf{s}_{12} is τ/g_{1b} with $\alpha = 1 - \frac{\tau}{g_{1b} P_1}$. Meanwhile, U2’s messages are not supposed to be decoded firstly for covertness, which results in $\alpha P_1 \geq 0$, i.e., $P_1 \geq \tau/g_{1b}$. The target rates of \mathbf{s}_{12} and \mathbf{s}_{11} are set as $\hat{R}_{12} = \log_2(1 + \frac{\tau}{\sigma_b^2})$ and $\hat{R}_{11} = \hat{R}_1 - \hat{R}_{12}$, respectively. The power allocation scheme and decoding order are shown in Figure 2b.

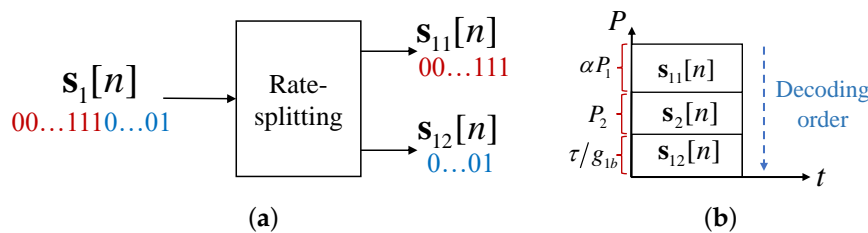


Figure 2. (a) A sample for splitting \mathbf{s}_1 into \mathbf{s}_{11} and \mathbf{s}_{12} . (b) An illustration of power allocation and decoding order.

2.3. Detection Metrics at Willie

Willie tries to make a decision whether U2 is transmitting or not based on the received signals $\mathbf{y}_w[n]$. From the independent and identically distributed (i.i.d.) nature of Willie’s received signals, the distribution of $\mathbf{y}_w[n]$ is expressed as

$$\begin{cases} \mathcal{CN}(0, g_{1w}P_1 + \sigma_w^2), & \mathcal{H}_0, \\ \mathcal{CN}(0, g_{1w}P_1 + g_{2w}P_2 + \sigma_w^2), & \mathcal{H}_1. \end{cases} \tag{5}$$

According to the Neyman-Pearson criterion, the optimal decision rule at Willie is the likelihood ratio test (LRT) [14,15], which can be shown as a radiometer

$$T_w \underset{\mathcal{D}_1}{\overset{\mathcal{D}_0}{\gtrless}} \lambda, \tag{6}$$

where $T_w = \frac{1}{N} \sum_{n=1}^N |\mathbf{y}_w[n]|^2$ is the average power received at Willie in a time slot, λ is the detection threshold of Willie, \mathcal{D}_1 and \mathcal{D}_0 are the binary decisions for the hypotheses \mathcal{H}_0 and \mathcal{H}_1 , respectively. Considering a long observation of Willie, i.e., $N \rightarrow \infty$, and employing the strong law of large numbers, i.e., $\chi_{2N}^2/N \rightarrow 1$, T_w is given by

$$\begin{aligned} T_w &= \lim_{N \rightarrow \infty} \begin{cases} (g_{1w}P_1 + \sigma_w^2)\chi_{2N}^2/N, & \mathcal{H}_0, \\ (g_{1w}P_1 + g_{2w}P_2 + \sigma_w^2)\chi_{2N}^2/N, & \mathcal{H}_1, \end{cases} \\ &= \begin{cases} g_{1w}P_1 + \sigma_w^2, & \mathcal{H}_0, \\ g_{1w}P_1 + g_{2w}P_2 + \sigma_w^2, & \mathcal{H}_1. \end{cases} \end{aligned} \tag{7}$$

The detection performance is measured by the DEP, which is denoted as

$$\mathbb{P}_E \triangleq \mathbb{P}_{FA} + \mathbb{P}_{MD}, \tag{8}$$

where $\mathbb{P}_{FA} = \mathbb{P}\{T_w > \lambda | \mathcal{H}_0\}$ is the false alarm probability (FAP), $\mathbb{P}_{MD} = \mathbb{P}\{T_w < \lambda | \mathcal{H}_1\}$ is the miss detection probability (MDP), $\mathbb{P}\{\cdot\}$ denotes probability operation and the prior probabilities of hypotheses \mathcal{H}_0 and \mathcal{H}_1 are assumed to be equal, i.e., $\mathbb{P}(\mathcal{H}_0) = \mathbb{P}(\mathcal{H}_1) = 1/2$.

3. Performance Analysis

In this section, we analyze the performances of the covertness and sum rate in the proposed system.

3.1. Covertness Analysis

Similar to the proof in [21], the FAP and DEP are given by

$$\mathbb{P}_{FA} = \begin{cases} 1, & \frac{\lambda - \sigma_w^2}{g_{1w}} < p_1^{\min}, \\ \frac{g_{1w}p_1^{\max} + \sigma_w^2 - \lambda}{g_{1w}(p_1^{\max} - p_1^{\min})}, & p_1^{\min} \leq \frac{\lambda - \sigma_w^2}{g_{1w}} \leq p_1^{\max}, \\ 0, & \frac{\lambda - \sigma_w^2}{g_{1w}} > p_1^{\max}, \end{cases} \tag{9}$$

$$\mathbb{P}_{MD} = \begin{cases} 0, & \frac{\lambda - \sigma_w^2}{g_{1w}} < \rho_1, \\ \frac{\lambda - g_{1w}p_1^{\min} - g_{2w}P_2 - \sigma_w^2}{g_{1w}(p_1^{\max} - p_1^{\min})}, & \rho_1 \leq \frac{\lambda - \sigma_w^2}{g_{1w}} \leq \rho_2, \\ 1, & \frac{\lambda - \sigma_w^2}{g_{1w}} > \rho_2, \end{cases} \tag{10}$$

where $\rho_1 = P_1^{\min} + \frac{g_{2w}}{g_{1w}} P_2$, $\rho_2 = P_1^{\max} + \frac{g_{2w}}{g_{1w}} P_2$. Then, the DEP at Willie is given by

$$\mathbb{P}_E = \begin{cases} 1, & \frac{\lambda - \sigma_w^2}{g_{1w}} < P_1^{\min}, \\ \frac{g_{1w} P_1^{\max} + \sigma_w^2 - \lambda}{g_{1w} (P_1^{\max} - P_1^{\min})}, & P_1^{\min} \leq \frac{\lambda - \sigma_w^2}{g_{1w}} < \rho_1, \\ 1 - \frac{g_{2w} P_2}{g_{1w} (P_1^{\max} - P_1^{\min})}, & \rho_1 \leq \frac{\lambda - \sigma_w^2}{g_{1w}} \leq P_1^{\max}, \\ \frac{\lambda - g_{1w} P_1^{\min} - g_{2w} P_2 - \sigma_w^2}{g_{1w} (P_1^{\max} - P_1^{\min})}, & P_1^{\max} < \frac{\lambda - \sigma_w^2}{g_{1w}} \leq \rho_2, \\ 1, & \frac{\lambda - \sigma_w^2}{g_{1w}} > \rho_2. \end{cases} \quad (11)$$

Note that the condition $g_{1w} (P_1^{\max} - P_1^{\min}) \geq g_{2w} P_2$ needs to be satisfied; otherwise, Willie has zero probability of making detection errors.

According to the monotonicity of (11), the minimum DEP is given by

$$\mathbb{P}_E^\dagger = 1 - \frac{g_{2w} P_2}{g_{1w} (P_1^{\max} - P_1^{\min})}, \quad (12)$$

and the corresponding detection threshold satisfies $\rho_1 \leq \frac{\lambda - \sigma_w^2}{g_{1w}} \leq P_1^{\max}$. Since legitimate users don't have instantaneous CSI between Willie and U2, we consider the expected minimum DEP $\overline{\mathbb{P}_E^\dagger}$ over all possible realization of h_{2w} as the measurement of covertness from the perspective of legitimate users. $\overline{\mathbb{P}_E^\dagger}$ is given by

$$\begin{aligned} \overline{\mathbb{P}_E^\dagger} &= \int_0^{\frac{g_{1w} (P_1^{\max} - P_1^{\min})}{P_2}} \mathbb{P}_E^\dagger f_{g_{2w}}(x) dx \\ &= \int_0^{\frac{g_{1w} (P_1^{\max} - P_1^{\min})}{P_2}} \left[1 - \frac{x P_2}{g_{1w} (P_1^{\max} - P_1^{\min})} \right] \frac{1}{L_{2w}} e^{-\frac{x}{L_{2w}}} dx \\ &= 1 + \frac{L_{2w} P_2}{g_{1w} (P_1^{\max} - P_1^{\min})} \left[e^{-\frac{g_{1w} (P_1^{\max} - P_1^{\min})}{L_{2w} P_2}} - 1 \right], \end{aligned} \quad (13)$$

where $f_{g_{2w}}(x)$ is the probability density function of g_{2w} .

The results indicate that as the variation interval of P_1 increases, there is a corresponding rise in DEP, leading to a larger value of \hat{R}_2 . In addition, U1 can modify its channel to Willie by repositioning to meet the covertness requirement.

3.2. Sum Rate Analysis

In the proposed scheme, the power allocation for \mathbf{s}_{12} is designed to prevent connection outages during the decoding of both \mathbf{s}_2 and \mathbf{s}_{12} . However, an outage may still occur during the decoding of \mathbf{s}_{11} due to the randomness of P_1 . Therefore, the outage probability of the system is determined by that of decoding \mathbf{s}_{11} . We respectively analyze the outage probabilities and ESR under \mathcal{H}_0 and \mathcal{H}_1 in the following.

1. Under \mathcal{H}_1

The achievable rate under \mathcal{H}_1 of \mathbf{s}_{11} is given by

$$R_{11}^1 = \log_2 \left(1 + \frac{g_{1b} P_1 - \tau}{g_{2b} P_2 + \tau + \sigma_b^2} \right). \quad (14)$$

Thus, the outage probability of s_{11} under \mathcal{H}_1 is expressed as

$$\begin{aligned} \mathbb{O}_{11}^1 &= \mathbb{P}\{R_{11}^1 < \hat{R}_{11}\} \\ &= \mathbb{P}\left\{P_1 < \frac{\mu_{11}(g_{2b}P_2 + \tau + \sigma_b^2) + \tau}{g_{1b}}\right\} \\ &= \max\left\{\frac{\mu_{11}(g_{2b}P_2 + \tau + \sigma_b^2) + \tau - g_{1b}P_1^{\min}}{g_{1b}(P_1^{\max} - P_1^{\min})}, 0\right\}, \end{aligned} \tag{15}$$

where $\mu_{11} = 2^{\hat{R}_{11}} - 1$. Eventually, the ESR under \mathcal{H}_1 is given by

$$\bar{R}_{\text{sum}}^1 = (\hat{R}_{11} + \hat{R}_2 + \hat{R}_{12})(1 - \mathbb{O}_{11}^1). \tag{16}$$

2. Under \mathcal{H}_0

Similarly, the achievable rate under \mathcal{H}_0 of s_{11} is given by

$$R_{11}^1 = \log_2\left(1 + \frac{g_{1b}P_1 - \tau}{\tau + \sigma_b^2}\right). \tag{17}$$

And the outage probability of s_{11} under \mathcal{H}_0 is expressed as

$$\begin{aligned} \mathbb{O}_{11}^0 &= \mathbb{P}\{R_{11}^0 < \hat{R}_{11}\} \\ &= \mathbb{P}\left\{P_1 < \frac{\mu_{11}(\tau + \sigma_b^2) + \tau}{g_{1b}}\right\} \\ &= \max\left\{\frac{\mu_{11}(\tau + \sigma_b^2) + \tau - g_{1b}P_1^{\min}}{g_{1b}(P_1^{\max} - P_1^{\min})}, 0\right\}. \end{aligned} \tag{18}$$

Since fixed power is allocated to s_{12} to satisfy \hat{R}_{12} , $\mathbb{P}\{R_{11}^0 < \hat{R}_{11}\} = \mathbb{P}\{R_1^0 < \hat{R}_1\}$. The ESR under \mathcal{H}_0 is given by

$$\bar{R}_{\text{sum}}^0 = (\hat{R}_{11} + \hat{R}_{12})(1 - \mathbb{O}_{11}^0). \tag{19}$$

Finally, the ESR of the system is expressed as

$$\begin{aligned} \bar{R}_{\text{sum}} &= \frac{1}{2}(\bar{R}_{\text{sum}}^0 + \bar{R}_{\text{sum}}^1) \\ &\triangleq f\left[(a - b2^{\hat{R}_{11}})\hat{R}_{11} - c2^{\hat{R}_{11}} + d\right], \end{aligned} \tag{20}$$

where $a = 2g_{1b}P_1^{\max} + g_{2b}P_2 + 2\sigma_b^2$, $b = g_{2b}P_2 + 2\tau + 2\sigma_b^2$, $c = (2\hat{R}_{12} + \hat{R}_2)(\tau + \sigma_b^2) + (\hat{R}_{12} + \hat{R}_2)g_{2b}P_2$, $d = (2\hat{R}_{12} + \hat{R}_2)(g_{1b}P_1^{\max} + \sigma_b^2) + (\hat{R}_{12} + \hat{R}_2)g_{2b}P_2$, and $f = \frac{1}{2g_{1b}(P_1^{\max} - P_1^{\min})}$. Component 1/2 is due to $\mathbb{P}(\mathcal{H}_0) = \mathbb{P}(\mathcal{H}_1) = 1/2$.

Equation (20) demonstrates that as \hat{R}_{11} increases, the outage probabilities also increase, whereas the change in ESR is uncertain. Therefore, to maximize ESR, it is necessary to consider how to set \hat{R}_{11} .

Lemma 1. The optimal \hat{R}_{11} to maximize the ESR is given by

$$\hat{R}_{11}^\dagger = \max\left\{0, \log_2 e \left[W\left(\frac{ae^{2c/b}}{b}\right) - 1 \right] - \frac{c}{b} \right\}, \tag{21}$$

where e is Euler's number, and $W(\cdot)$ denotes Lambert W Function [22]. The corresponding \bar{R}_{sum} is denoted as $\bar{R}_{\text{sum}}(\hat{R}_{11}^\dagger)$.

Proof. See Appendix A. \square

We notice that as g_{1w} increases, \hat{R}_{11}^\dagger increases, resulting in a higher ESR. Therefore, ESR can be increased by placing U1 closer to the BS.

4. Optimization Problem

In this letter, we aim to maximize the ESR by optimizing the deployment of U1 and the target rate of s_{11} , subject to the covertness constraint and the ECR constraint. The optimization problem is formulated as

$$\max_{x_1, y_1, \hat{R}_{11}} \bar{R}_{\text{sum}}, \tag{22a}$$

$$\text{s.t. } \bar{\mathbb{P}}_E^\dagger \geq 1 - \delta, \tag{22b}$$

$$\bar{R}_2 = \hat{R}_2(1 - \mathbb{O}_{11}^1) \geq \epsilon, \tag{22c}$$

where (22b) is the covertness constraint, and (22c) is the ECR constraint. To solve the optimization problem (22), we decompose it into two subproblems, as shown in Figure 3. We first discuss the monotonicity of \bar{R}_{sum} , $\bar{\mathbb{P}}_E$, and \bar{R}_2 w.r.t. x_1 and y_1 . We observe that as the distance between U1 and Bob, i.e., $\|\mathbf{q}_1 - \mathbf{q}_b\|$, decreases, both \bar{R}_{sum} and \bar{R}_2 increases. On the other hand, $\bar{\mathbb{P}}_E$ decreases since U1 gets farther away from Willie. Then, the first subproblem is to optimize the placement of U1 under the covertness constraint (22b) to minimize the distance between U1 and Bob. The second subproblem is to optimize \hat{R}_{11} under the ECR constraint (22c) and U1’s optimal placement obtained from the first subproblem to maximize the ESR.

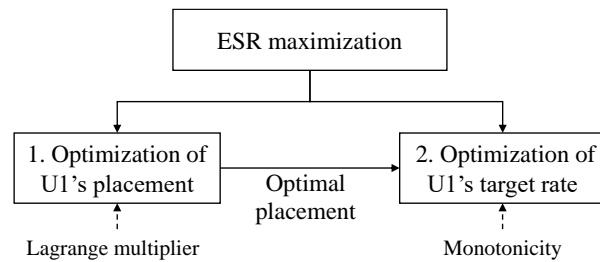


Figure 3. Procedure for solving optimization problem (22).

The first subproblem to optimize U1’s placement is expressed as

$$\min_{x_1, y_1} x_1^2 + y_1^2, \tag{23a}$$

$$\text{s.t. } (x_1 - x_w)^2 + (y_1 - y_w)^2 \leq t, \tag{23b}$$

$$t = \frac{\delta \beta_0 (P_1^{\text{max}} - P_1^{\text{min}})}{g_{2w} P_2 \left[1 + W\left(-\frac{e^{-1/\delta}}{\delta}\right) \right]} - z_1^2. \tag{23c}$$

Lemma 2. The optimal position of U1 is given by $\mathbf{q}_1^\dagger = [x_1^\dagger, y_1^\dagger, z_1]$ when $0 < t < x_w^2 + y_w^2$, where $[x_1^\dagger, y_1^\dagger] = \left(1 - \sqrt{\frac{t}{x_w^2 + y_w^2}}\right)[x_w, y_w]$, otherwise, $x_1^\dagger = y_1^\dagger = 0$, when $t \geq x_w^2 + y_w^2$.

Proof. See Appendix B. \square

From Lemma 2, we notice that the optimal horizontal position of U1 lies on the line between BS and Willie.

The second subproblem to optimize \hat{R}_{11} is expressed as

$$\max_{\hat{R}_{11}} \bar{R}_{\text{sum}}(x_1^\dagger, y_1^\dagger), \tag{24a}$$

$$\text{s.t. } \mathbb{O}_{11}(x_1^\dagger, y_1^\dagger) \leq 1 - \frac{\epsilon}{\hat{R}_2}, \tag{24b}$$

where $\bar{R}_{\text{sum}}(x_1^\dagger, y_1^\dagger)$ and $\mathbb{O}_{11}(x_1^\dagger, y_1^\dagger)$ represent substituting $(x_1^\dagger, y_1^\dagger)$ into \bar{R}_{sum} and \mathbb{O}_{11} , respectively. It is shown in (18) that \mathbb{O}_{11} is a monotonically increasing function w.r.t. \hat{R}_{11} . Thus, the upper limit of \hat{R}_{11} is expressed as \hat{R}_{11}^ϵ , where \hat{R}_{11}^ϵ is the solution of $\mathbb{O}_{11}(x_1^\dagger, y_1^\dagger) = 1 - \frac{\epsilon}{\hat{R}_2}$.

Together with Lemma 1, the optimal choice of \hat{R}_{11} is given by $\hat{R}_{11}^\dagger = \min\{\hat{R}_{11}^\epsilon, \hat{R}_{11}^\dagger\}$.

5. Numerical Results

In this section, we present numerical results to investigate the performance of the proposed covert communication scheme. Unless otherwise stated, we set $\beta_0 = -20$ dB, $\mathbf{q}_b = [0, 0, 10]$ m, $\mathbf{q}_w = [0, 100, 0]$ m, $\mathbf{q}_2 = [50, 50, 0]$ m, $z_1 = 25$ m, $P_1^{\text{max}} = 10$ W, $P_1^{\text{min}} = 1$ W, $P_2 = 2$ W, $\sigma_b^2 = \sigma_w^2 = -60$ dBm. In this section, we compared the proposed method with NOMA systems, which can be regarded as a special case of RSMA where all power is allocated to \mathbf{s}_{11} .

Figure 4 shows the maximum ESR versus the expected minimum DEP with different ECR constraints in RSMA and NOMA systems, where $\hat{R}_2 = 3$ bpcu. We observe that the curves remain stable initially, but decrease as the expected minimum DEP increases. When the covertness constraint is loose ($t \geq x_w^2 + t_w^2$), the placement of U1 remains unchanged at $x_1 = y_1 = 0$. As the covertness constraint increases, U1 moves closer to Willie while moving further from the BS, thereby leading to a decrement in ESR. Additionally, a higher ECR constraint results in a lower ESR, implying that \mathbb{O}_{11}^1 is not zero at the maximum ESR. Moreover, the proposed scheme has a higher ESR than NOMA with the same minimum DEP.

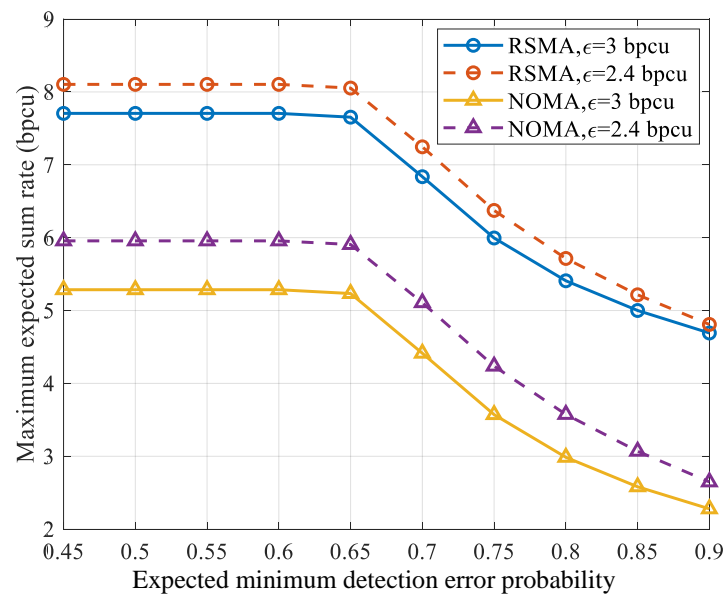


Figure 4. The maximum ESR versus the expected minimum DEP for different ECR constraints in RSMA and NOMA systems, where $\hat{R}_2 = 3$ bpcu.

Figure 5 depicts \mathbb{O}_{11}^1 of \hat{R}_{11}^\dagger versus \hat{R}_2 for different covertness constraints in RSMA and NOMA systems. In this case, we do not consider the ESR constraint. We find that NOMA has a higher outage probability than RSMA to maximize the ESR. Moreover, as \hat{R}_2 increases, the \mathbb{O}_{11}^1 of RSMA increases, while that of NOMA decreases. When $\tau = 0$ (i.e., at maximum \hat{R}_2), the \mathbb{O}_{11}^1 of both systems are equal. In NOMA systems, fixed power is allocated to \mathbf{s}_{11} ($\alpha = 1$). As \hat{R}_2 increases, decreasing \mathbb{O}_{11}^1 to increase \bar{R}_2 will result in a larger ESR. In RSMA

systems, with the increment of \hat{R}_2 , more power is allocated to s_{11} , and more outages can be tolerated to increase the ESR.

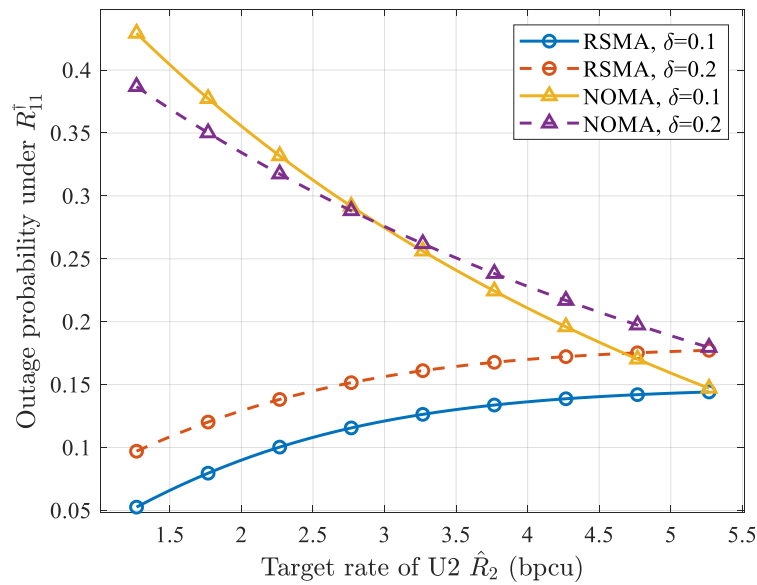


Figure 5. The outage probability of \hat{R}_{11}^+ under \mathcal{H}_1 for different covertness constraints in RSMA and NOMA systems, where $\epsilon = 0.8\hat{R}_2$.

Figure 6 plots the maximum ESR versus \hat{R}_2 for different covertness constraints, where $\epsilon = 0.8\hat{R}_2$. Similar to Figure 5, we observe that the maximum ESR of RSMA increases while that of NOMA decreases as \hat{R}_2 increases. Specifically, when the covertness constraint is looser, RSMA achieves a higher \mathbb{O}_{11}^1 and ESR compared to NOMA. This can be attributed to the fact that the channel gain between the BS and U1 is stronger. The stronger channel gain results in R_1 playing a more crucial role in determining ESR, thus leading to an increase in \mathbb{O}_{11}^1 .

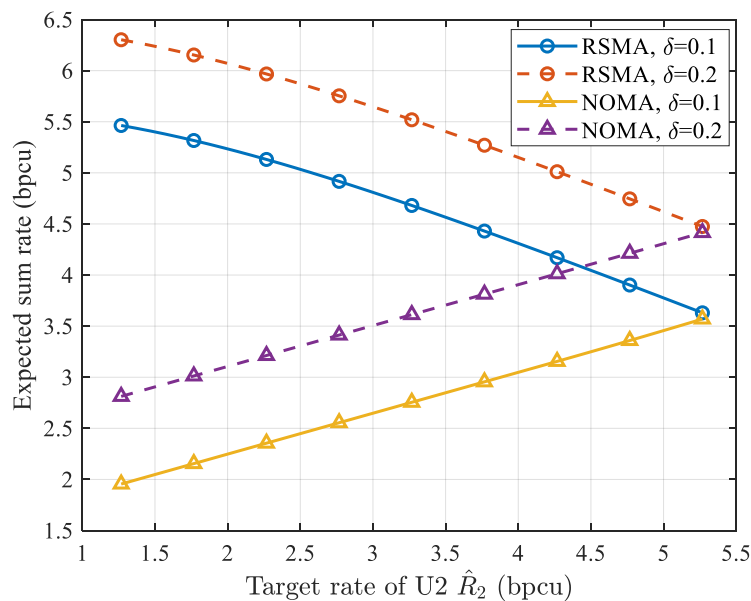


Figure 6. The maximum ESR versus the target rate of U2 \hat{R}_2 for different covertness constraints in RSMA and NOMA systems, where $\epsilon = 0.8\hat{R}_2$.

6. Conclusions

In this paper, we investigated the covert communication in UAV-assisted uplink RSMA system, where U1 adopts an RS strategy with random transmit power to guarantee U2's covert and reliable transmission. Specially, we studied the optimal power allocation factor for s_{11} and s_{12} . Then, we derived closed-form expressions of minimum DEP, ESR, and UAV's optimal target rate that maximizes ESR. Constrained by the minimum DEP and ECR, we maximized the ESR by optimizing the position and target rate of the UAV. Numerical results showed that the proposed scheme outperforms NOMA systems in terms of the ESR constraint by the same DEP and ECR.

Author Contributions: Conceptualization, Z.D. and X.Y.; methodology, Z.D.; software, Z.D.; validation, Z.D.; formal analysis, Z.D.; investigation, Z.D.; data curation, Z.D.; writing—original draft preparation, Z.D.; writing—review and editing, Z.D, X.Y. and L.W.; visualization, Z.D.; supervision, X.Y.; project administration, L.W. and T.Z.; funding acquisition, L.W., T.Z. and X.Y. All authors have read and agreed to the published version of the manuscript.

Funding: This work was supported in part by the National Natural Science Foundation of China under Grant No. 62271412, 62271399, and partly supported by Natural Science Basic Research Plan in Shaanxi Province of China under grant No. 2022KJXX-39.

Institutional Review Board Statement: Not applicable.

Informed Consent Statement: Not applicable.

Data Availability Statement: Not applicable.

Conflicts of Interest: The authors declare no conflict of interest.

Abbreviations

The following abbreviations are used in this manuscript:

PLS	Physical layer security
AWGN	Additive white Gaussian noise
UAV	Unmanned aerial vehicle
RSMA	Rate-splitting multiple access
NOMA	Non-orthogonal multiple access
RS	Rate-splitting
BS	Base station
ESR	Expected sum rate
DEP	Detection error probability
3D	Three-dimensional
CSI	Channel state information
LOS	Line-of-sight
SINR	Signal-to-interference-plus-noise ratio
LRT	Likelihood ratio test
FAP	False alarm probability
MDP	Miss detection probability
KKT	Karush–Kuhn–Tucker

Appendix A. Proof of Lemma 1

Taking the derivative of (20) w.r.t. \hat{R}_{11} yields

$$\frac{\partial \bar{R}_{\text{sum}}}{\partial \hat{R}_{11}} = f \left\{ a - [b + (c + b\hat{R}_{11}) \log_e 2] 2^{\hat{R}_{11}} \right\}. \quad (\text{A1})$$

By setting $\frac{\partial \bar{R}_{\text{sum}}}{\partial \hat{R}_{11}} = 0$, we have

$$\begin{aligned} a - [b + (c + b\hat{R}_{11}) \log_e 2] 2^{\hat{R}_{11}} &= 0 \\ \left[1 + \left(\frac{c}{b} + \hat{R}_{11}\right) \log_e 2\right] e^{[1 + (\frac{c}{b} + \hat{R}_{11}) \log_e 2]} &= \frac{ae2^{c/b}}{b}. \end{aligned} \quad (\text{A2})$$

According to the definition of Lambert W Function, i.e., $x = W(v)$ is the solution of $xe^x = v (v \geq 0)$, (A2) can be rephrased as

$$\begin{aligned} 1 + \left(\frac{c}{b} + \hat{R}_{11}\right) \log_e 2 &= W\left(\frac{ae2^{c/b}}{b}\right) \\ \hat{R}_{11} &= \log_2 e \left[W\left(\frac{ae2^{c/b}}{b}\right) - 1 \right] - \frac{c}{b}. \end{aligned} \quad (\text{A3})$$

It is obviously that \bar{R}_{sum} is a concave function since (A1) is monotonically decreasing w.r.t \hat{R}_{11} . Therefore, the solution of (A3) is a maximum point. In addition, \hat{R}_{11} should be no less than 0, which completes the proof.

Appendix B. Proof of Lemma 2

The Lagrangian of this problem is

$$L(x_1, y_1, \kappa) = x_1^2 + y_1^2 + \kappa[(x_1 - x_w)^2 + (y_1 - y_w)^2 - t]. \quad (\text{A4})$$

Taking the derivative of L w.r.t to x_1 and y_1 obtains the Karush–Kuhn–Tucker (KKT) conditions

$$2x_1 + 2\kappa(x_1 - x_w) = 0, \quad (\text{A5a})$$

$$2y_1 + 2\kappa(y_1 - y_w) = 0, \quad (\text{A5b})$$

$$\kappa[(x_1 - x_w)^2 + (y_1 - y_w)^2 - t] = 0, \quad (\text{A5c})$$

$$(x_1 - x_w)^2 + (y_1 - y_w)^2 \leq t \quad (\text{A5d})$$

$$\kappa \geq 0. \quad (\text{A5e})$$

When $\kappa = 0$, it's obvious that $x_1^\dagger = y_1^\dagger = 0$. Meanwhile, to satisfy (A5d), one obtains $t \geq x_w^2 + y_w^2$.

When $\kappa > 0$, after some manipulations, we have $x_1^\dagger = \frac{\kappa x_w}{1+\kappa}$, $y_1^\dagger = \frac{\kappa y_w}{1+\kappa}$, $\kappa = -1 + \sqrt{\frac{x_w^2 + y_w^2}{t}}$, and $0 < t < x_w^2 + y_w^2$. The proof is completed.

References

1. Wang, D.; He, T.; Zhou, F.; Cheng, J.; Zhang, R.; Wu, Q. Outage-driven link selection for secure buffer-aided networks. *Sci. China-Inf. Sci.* **2022**, *65*, 1–16. [CrossRef]
2. Lin, Z.; Lin, M.; Champagne, B.; Zhu, W.P.; Al-Dhahir, N. Secrecy-Energy Efficient Hybrid Beamforming for Satellite-Terrestrial Integrated Networks. *IEEE Trans. Commun.* **2021**, *69*, 6345–6360. [CrossRef]
3. Bash, B.A.; Goeckel, D.; Towsley, D. Limits of Reliable Communication with Low Probability of Detection on AWGN Channels. *IEEE J. Sel. Top. Signal Process.* **2013**, *31*, 1921–1930. [CrossRef]
4. Sobers, T.V.; Bash, B.A.; Guha, S.; Towsley, D.; Goeckel, D. Covert Communication in the Presence of an Uninformed Jammer. *IEEE Trans. Wirel. Commun.* **2017**, *16*, 6193–6206. [CrossRef]
5. Wang, D.; Zhou, F.; Lin, W.; Ding, Z.; Al-Dhahir, N. Cooperative Hybrid Non-orthogonal Multiple Access-Based Mobile-Edge Computing in Cognitive Radio Networks. *IEEE Trans. Cogn. Commun. Netw.* **2022**, *8*, 1104–1117. [CrossRef]
6. Lin, Z.; Lin, M.; Wang, J.B.; de Cola, T.; Wang, J. Joint Beamforming and Power Allocation for Satellite-Terrestrial Integrated Networks With Non-Orthogonal Multiple Access. *IEEE J. Sel. Top. Signal Process.* **2019**, *13*, 657–670. [CrossRef]
7. Wang, D.; Wu, M.; He, Y.; Pang, L.; Xu, Q.; Zhang, R. An HAP and UAVs Collaboration Framework for Uplink Secure Rate Maximization in NOMA-Enabled IoT Networks. *Remote Sens.* **2022**, *14*, 4501. [CrossRef]

8. Zhou, G.; Mao, Y.; Clerckx, B. Rate-Splitting Multiple Access for Multi-Antenna Downlink Communication Systems: Spectral and Energy Efficiency Tradeoff. *IEEE Trans. Wirel. Commun.* **2022**, *21*, 4816–4828. [[CrossRef](#)]
9. Li, X.; Fan, Y.; Yao, R.; Wang, P.; Qi, N.; Miridakis, N.I.; Tsiftsis, T.A. Rate-Splitting Multiple Access-Enabled Security Analysis in Cognitive Satellite Terrestrial Networks. *IEEE Trans. Veh. Technol.* **2022**, *71*, 11756–11771. [[CrossRef](#)]
10. Liu, H.; Bai, Z.; Lei, H.; Pan, G.; Kim, K.J.; Tsiftsis, T.A. A New Rate Splitting Strategy for Uplink CR-NOMA Systems. *IEEE Trans. Veh. Technol.* **2022**, *71*, 7947–7951. [[CrossRef](#)]
11. Yang, Z.; Chen, M.; Saad, W.; Xu, W.; Shikh-Bahaei, M. Sum-Rate Maximization of Uplink Rate Splitting Multiple Access (RSMA) Communication. *IEEE Trans. Mob. Comput.* **2022**, *21*, 2596–2609. [[CrossRef](#)]
12. Lin, Z.; Lin, M.; de Cola, T.; Wang, J.B.; Zhu, W.P.; Cheng, J. Supporting IoT With Rate-Splitting Multiple Access in Satellite and Aerial-Integrated Networks. *IEEE Internet Things J.* **2021**, *8*, 11123–11134. [[CrossRef](#)]
13. Lin, Z.; Lin, M.; Champagne, B.; Zhu, W.P.; Al-Dhahir, N. Secure and Energy Efficient Transmission for RSMA-Based Cognitive Satellite-Terrestrial Networks. *IEEE Wirel. Commun. Lett.* **2021**, *10*, 251–255. [[CrossRef](#)]
14. Wang, M.; Yang, W.; Lu, X.; Hu, C.; Liu, B.; Lv, X. Channel Inversion Power Control Aided Covert Communications in Uplink NOMA Systems. *IEEE Wirel. Commun. Lett.* **2022**, *11*, 871–875. [[CrossRef](#)]
15. Lv, L.; Wu, Q.; Li, Z.; Ding, Z.; Al-Dhahir, N.; Chen, J. Covert Communication in Intelligent Reflecting Surface-Assisted NOMA Systems: Design, Analysis, and Optimization. *IEEE Trans. Wirel. Commun.* **2022**, *21*, 1735–1750. [[CrossRef](#)]
16. Yan, S.; Hanly, S.V.; Collings, I.B. Optimal Transmit Power and Flying Location for UAV Covert Wireless Communications. *IEEE J. Sel. Areas Commun.* **2021**, *39*, 3321–3333. [[CrossRef](#)]
17. Rao, H.; Xiao, S.; Yan, S.; Wang, J.; Tang, W. Optimal Geometric Solutions to UAV-Enabled Covert Communications in Line-of-Sight Scenarios. *IEEE Trans. Wirel. Commun.* **2022**, *21*, 10633–10647. [[CrossRef](#)]
18. Su, Y.; Fu, S.; Si, J.; Xiang, C.; Zhang, N.; Li, X. Optimal Hovering Height and Power Allocation for UAV-aided NOMA Covert Communication System. *IEEE Wirel. Commun. Lett.* **2023**, 1–5. [[CrossRef](#)]
19. 3GPP. *Technical Specification Group Radio Access Network; Study on Channel Model for Frequencies from 0.5 to 100 GHz (Release 14); Technical Specification (TS) 38.901; Version 14.3.0; 3rd Generation Partnership Project (3GPP)*. 2018. Available online: [drones-2295032pleaseconfirmthis.Ifthereisnolocation,pleaseaddthewebsiteandaccesseddatehttps://www.etsi.org/deliver/etsi_tr/138900_138999/138901/14.00.00_60/tr_138901v140000p.pdf](https://www.etsi.org/deliver/etsi_tr/138900_138999/138901/14.00.00_60/tr_138901v140000p.pdf) (accessed on 6 March 2023).
20. Zhou, X.; Yan, S.; Shu, F.; Chen, R.; Li, J. UAV-Enabled Covert Wireless Data Collection. *IEEE J. Sel. Areas Commun.* **2021**, *39*, 3348–3362. [[CrossRef](#)]
21. Shahzad, K.; Zhou, X.; Yan, S.; Hu, J.; Shu, F.; Li, J. Achieving Covert Wireless Communications Using a Full-Duplex Receiver. *IEEE Trans. Wirel. Commun.* **2018**, *17*, 8517–8530. [[CrossRef](#)]
22. Corless, R.M.; Gonnet, G.H.; Hare, D.E.; Jeffrey, D.J.; Knuth, D.E. On the Lambert W function. *Adv. Comput. Math.* **1996**, *5*, 329–359. [[CrossRef](#)]

Disclaimer/Publisher’s Note: The statements, opinions and data contained in all publications are solely those of the individual author(s) and contributor(s) and not of MDPI and/or the editor(s). MDPI and/or the editor(s) disclaim responsibility for any injury to people or property resulting from any ideas, methods, instructions or products referred to in the content.